# Structural Performance of Concrete Encased Steel Columns with H-shaped Steel


**Junji SHI, Hiroshi KURAMOTO&Juan Jose CASTRO**
*Osaka University, Osaka Japan*

**Tomoya MATSUI**
*Toyohashi University of Technology, Toyohashi Japan*

**Toshiaki FUJIMOTO**
*Nihon University Tokyo, Japan*

**SUMMARY:**
The aim of this research is to evaluate the structural performance of the composite concrete encased steel (CES) columns, which are composed of H-shaped steel and fiber reinforced concrete. In this research program three phases of experiments were carried out on CES columns to evaluate their behaviour under cyclic loads. The parameters included the axial force ratio, the H-shaped steel ratio, the shear span ratio, the fiber contents ratio and the flange width of H-shaped steel. Also, a formulation that includes all these parameters for the evaluation of the deformation capacity was proposed and its validity was verified by comparing the calculated with the test results.

*Keywords: CES Columns, Fiber reinforced concrete, Static loading test, Deformation capacity*

## 1. INTRODUCTION

The steel reinforced concrete (SRC) construction system has been extensively used in Japan over the years. This structural system composed of steel and reinforced concrete has an excellent earthquake resistance in terms of strength and deformation capacity. However, the structural design process and construction works are more complicated than those for conventional reinforced concrete structures. The Concrete Encased Steel (CES) structural system, which consists of fiber reinforced concrete (FRC) and steel, without reinforcing bars, was proposed to solve these problems. According to the experiments that have been conducted in the past on columns and beam column joints, it is showed that the CES systems have restoring force characteristics comparable to the SRC system with good deformation capacity (Kuramoto et. al 2002, Fujimoto et. al 2008). Most of the experiments on columns were carried out using cross shape steel, while there are few experiments conducted on columns with H-shaped steel.

In this research, three phases of experiments were carried out on columns with H-shaped steel. The main parameters of Phase 1 were the axial load ratio, the steel ratio and the shear span ratio. The test results showed that CES columns with H-shaped steel had an excellent seismic behaviour. However, with the increase of the axial load ratio, the axial deformation became lager, and then local buckling of the steel flanges is more likely to occur after the maximum strength. In other words, the problem is how to keep the axial strength of the column. Then, to investigate the influence of the axial load ratio and the confining effect by band plate on local buckling of the steel flanges, the Phase 2 of experiments were performed using of axial load level and band plates' width as parameters. However the test results showed that band plates have little contribution to prevent the local buckling and the increase of the deformation capacity of the columns. As a reason, the collapse of the cover concrete and the smallness of confined concrete area can be mentioned. Therefore, to avoid the collapse and to delay the buckling of the steel, the Phase 3 of experiments, with increment of fiber contents ratio in FRC and flange width as parameter were carried out.

Based on the results of these three Phases of experiments, a formulation which encloses all the parameters (axial load ratio, steel ratio, shear span ratio, fiber contents ratio and flange width) for the evaluation of the deformation capacity is proposed and its validity was verified comparing the calculated with the test results.

## 2. EXPERIMENTAL PROGRAM

### 2.1 Specimens and Material Used

*2.1.1 Outline of Phase 1 Test*

A total of eight CES columns were tested. The details and dimensions of the specimens are shown in Table 2.1 and Fig.2.1. In this Phase, the columns had 300 mm square section for all specimens and different shear span ratios (2.5, 2.0, 1.5 and 1.0) were achieved by varying the column height (1500 mm, 1200 mm, 900 mm and 600 mm) to investigate the effect of shear span ratio on seismic behavior of the columns. The steel encased in the column had a single H-shaped steel of 200x150x6x9 mm for six of the specimens, while for the other two specimens of B3H and B3L, different dimension of 200x150x16x9 mm and 150x150x6x6 mm was used, respectively. FRC with poly vinyl alcohol (PVA) of 1.0% in the volume content ratio was used in all specimens. The mechanical properties of FRC and steel used are also listed in Table 2.1.

**Table 2.1** Test Plan of Phase 1

| Specimen | | | A2 | B1 | B2 | B3 | B3H | B3L | C2 | D2 |
|---|---|---|---|---|---|---|---|---|---|---|
| Reinforced fiber | | Fiber type | PVA fiber RF4000 | | | | | | | |
| | | Mixing volume (%) | 1.0% | | | | | | | |
| Cross section | | bxD (mm) | 300x300 | | | | | | | |
| Concrete strength | | $\sigma_B$ (N/mm$^2$) | 43.9 | 43.2 | 43.9 | 44.7 | 45.0 | 43.6 | 42.7 | 42.2 |
| Column height | | h (mm) | 1500 | 1200 | | | | | 900 | 600 |
| Shear span ratio | | a/D | 2.5 | 2.0 | | | | | 1.5 | 1.0 |
| Steel | Shape | | Single H-section | | | | | | | |
| | Cross section | | 200x150x6x9 | | | | 200x150x16x9 | 150x150x6x6 | 200x150x6x9 | |
| | Flange width ratio (bs/b) | | 0.5 | | | | | | | |
| | Yield stress | Flange (N/mm$^2$) | 277.7 | | | | | | | |
| | | Web (N/mm$^2$) | 279.4 | | | | | | | |
| Axial load | | N (kN) | 800 | 400 | 800 | 1200 | 1365 | 1130 | 800 | |
| Steel ratio | | As/bD | 4.21% | | | | 7.01% | 2.92% | 4.21% | |
| Axial load ratio | | $N/N_0$ | 0.188 | 0.095 | 0.188 | 0.28 | 0.30 | 0.292 | 0.192 | 0.193 |

$A_s$ : Sectional area of Steel

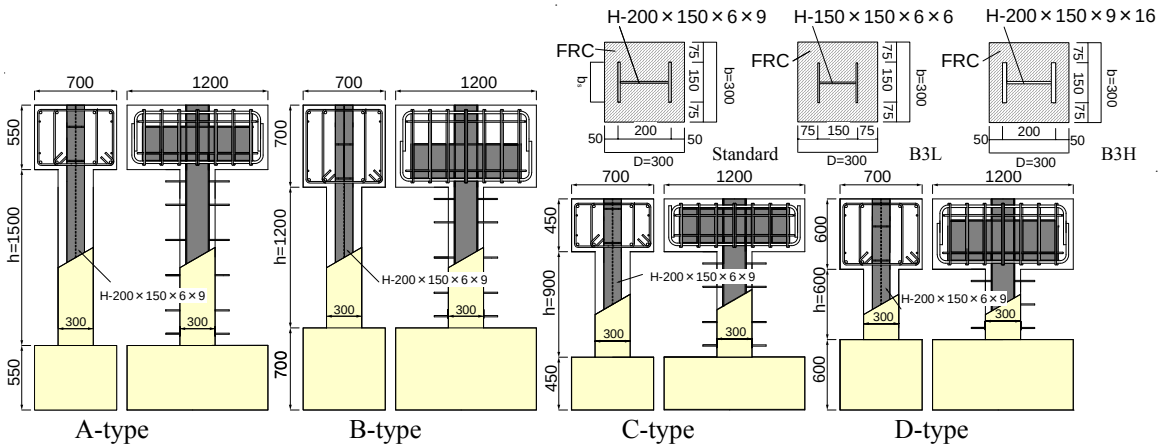


**Figure 2.1** Test specimen of Phase 1

*2.1.2 Outline of Phase 2 Test*

In this phase, five CES columns specimens were tested. The details and dimensions are shown in Table 2.2 and Fig. 2.2. All specimens had a column with 1200 mm height and 300 mm square section, and the encased steel was a single H-shaped of 200x150x6x9 mm. Five pieces of band plate were welded to the both sides of every H-shaped steel, except for Specimen B30-a. The width of all the

band plates for B30-b and B25-b was 50 mm, while for B30-c and B25-c, the band plate's width at top and bottom of column was 100 mm. FRC with the same kind of fiber and content as Phase 1 was used in this Phase. The mechanical properties of the materials used are listed in Table 2.2.

**Table 2.2** Test Plan of Phase 2

| Specimens | | | B30-a | B30-b | B30-c | B25-b | B25-c |
|---|---|---|---|---|---|---|---|
| Reinforced fiber | | Fiber type | PVA fiber RF4000 | | | | |
| | | Mixing volume (%) | 1.0% | | | | |
| Cross section | | bxD (mm) | 300x300 | | | | |
| Concrete strength | | $\sigma_B$ (N/mm$^2$) | 40.9 | 43.0 | 45.1 | 46.2 | 45.1 |
| Column height | | h (mm) | 1200 | | | | |
| Shear span ratio | | a/D | 2.0 | | | | |
| Steel | Shape | | Single H-shaped | | | | |
| | Cross section | | 200x150x6x9 (bs/b=0.5) | | | | |
| | Width of band plate | | No | 50mm | 50mm* | 50mm | 50mm* |
| | Yield stress | Flange (N/mm$^2$) | 322 | | | | |
| | | Web (N/mm$^2$) | 354 | | | | |
| | | Band plate | - | 341 | | | |
| Axial load | | N (kN) | 1200 | | | 1000 | |
| Steel ratio | | As/bD | 4.21% | | | | |
| Axial load ratio | | $N/N_0$ | 0.300 | | | 0.250 | |

*For B30-c and B25-c, the width of band plates at top and bottom of column are 100mm

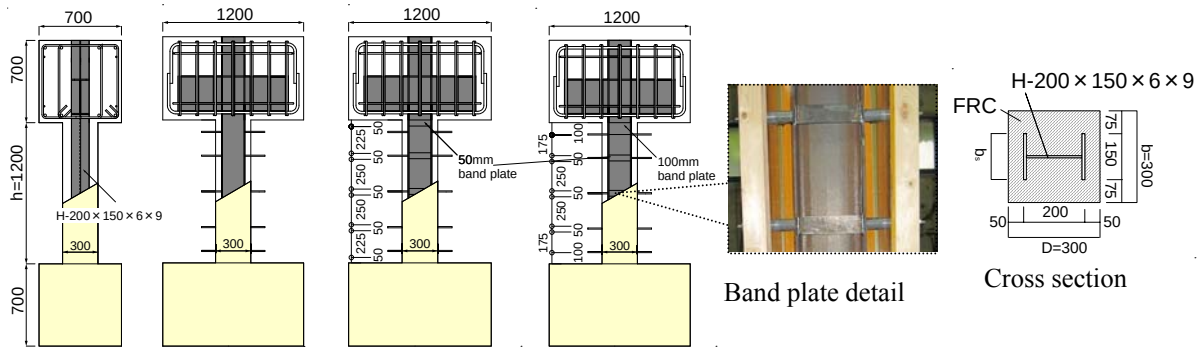


**Figure 2.2** Test specimen of Phase 2

*2.1.3 Outline of Phase 3 Test*

The details and dimensions of the three specimens tested in this phase are shown in Table 2.3 and Fig. 2.3. All specimens had a column with 1200 mm height and 300 mm square section same as Phase 2 test. The dimension of the single H-shaped steel encased in Specimen B3F was H-200x150x6x9 mm, and H-200x180x8x12 mm for B3MB and B3MB-F. The content of fiber mixed in the FRC was 1.0% for B3MB, while 1.5% for B3-F and B3MB-F. Also, Specimen B3 which tested in Phase 1 was added in Table 2.3 for comparison purpose.

**Table 2.3** Test Plan of Phase 3

| Specimens | | | B3 (phase 1) | B3-F | B3MB | B3MB-F |
|---|---|---|---|---|---|---|
| Reinforced fiber | | Fiber type | PVA fiber RF4000 | | | |
| | | Mixing volume (%) | 1.0% | 1.5% | 1.0% | 1.5% |
| Cross section | | bxD (mm) | 300x300 | | | |
| Concrete strength | | $\sigma_B$ (N/mm$^2$) | 44.7 | 33.6 | 36.4 | 34.7 |
| Column height | | h (mm) | 1200 | | | |
| Shear span ratio | | a/D | 2 | | | |
| Steel | Shape | | Single H-shaped | | | |
| | Cross section | | 200x150x6x9 | | 200x180x8x12 | |
| | Flange width ratio (bs/b) | | 0.5 | | 0.6 | |
| | Yield stress | Flange (N/mm$^2$) | 277.7 | 282.3 | 287.1 | |
| | | Web (N/mm$^2$) | 279.4 | 317.5 | 313.1 | |
| Axial load | | N (kN) | 1200 | 1000 | 1200 | 1160 |
| Steel ratio | | As/bD | 4.21% | | 6.36% | |
| Axial load ratio | | $N/N_0$ | 0.28 | | | |

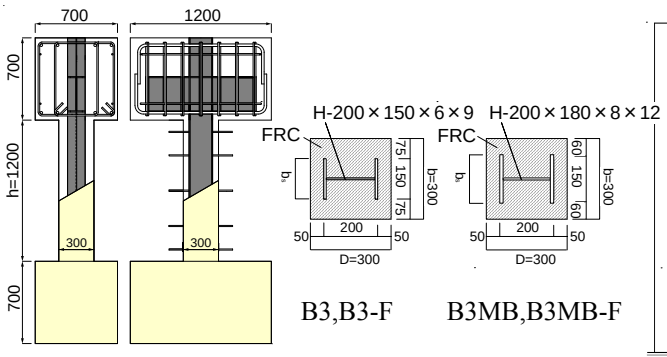


**Figure 2.3** Test specimen of Phase 3

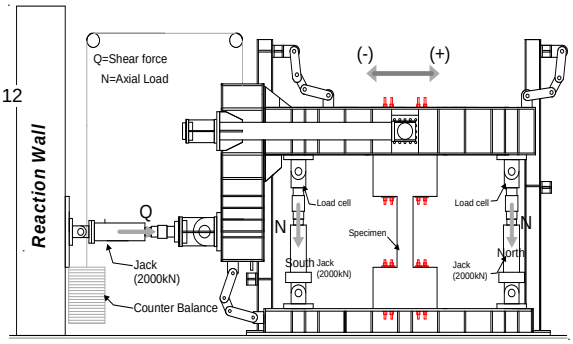


**Figure 2.4** Loading apparatus

## 2.2 Test Setup and Loading Procedures

All specimens were loaded with shear reversals by a horizontal hydraulic jack, and a constant axial load by two vertical hydraulic jacks, as shown in Fig. 2.4. The two vertical jacks applying constant axial compression were also used to keep the column top beam parallel to the bottom beam, so that the column is subjected to anti-symmetric moments. The incremental loading cycles were controlled by story drift angles, $R$, defined as the ratio of lateral displacements to the column height, $\delta/h$. The lateral load sequence consisted of one cycle to drift angle, $R$ of $0.25\times10^{-2}$ rad., followed by two cycles to each $R$ of $0.5\times10^{-2}$, $1.0\times10^{-2}$, $1.5\times10^{-2}$, $2.0\times10^{-2}$, $3.0\times10^{-2}$, $4.0\times10^{-2}$ rad., and then half for that of $5.0\times10^{-2}$rad., respectively. Furthermore, axial load ratio ($N/N_0$), axial load $N_0$ was calculated on the basis of SRC criterion as showed in Equations 2.1and 2.2.

$$N_0 = {}_c r_u \cdot \sigma_B \cdot {}_c A + {}_S \sigma_y \cdot {}_s A \quad (2.1)$$

$${}_c r_u = 0.85 - 2.5({}_s a_c / bD) \quad (2.2)$$

Where $N_o$: Axial strength of CES columns, ${}_cA$: Sectional area of concrete, ${}_sA$: Sectional area of Steel, ${}_c r_u$: Reduction factor of concrete and ${}_s a_c$: Sectional area of steel flange on compressive side.

## 3. EXPERIMENTAL RESULTS AND DISCUSSIONS

### 3.1. Experimental Results of Phase 1

Shear versus story drift angle relationships of Phase 1 test are shown in Fig. 3.1. Crack pattern of all specimens at the final loading stage are also presented in Photo 3.1.

In Specimens A2, B1 and B2, concentrated flexural cracks occurred at the end of columns. After reaching the maximum strength, spalling of cover concrete occurred at the top and bottom of columns, following with slight strength deterioration. Finally the specimens showed flexural failure.

In Specimens B3 and B3L, shear cracks were observed at story drift angle $R$ of $1.0\times10^{-2}$rad. After reaching the maximum strength, significant strength deterioration caused by the propagation of shear cracks from the top to bottom of columns was observed. In both specimens after concrete become severely damaged, the concrete contribution to axial load contributed, and the steel contribution increased.

In Specimen B3H with larger steel ratio, shear cracks occurred diagonally from the top to bottom of column at $R$ of $1.0\times10^{-2}$rad. The concrete was damaged greatly after $R$ of $2.0\times10^{-2}$rad. with the increase of axial strain. However, it sustained about 70% of the maximum strength at the final loading stage.

In Specimen C2, the maximum strength was attained at $R$ of $1.5\times10^{-2}$rad. Shear cracks at the top and bottom of column propagated while concrete compressive failure occurred at the top of column. Then, the column failed in shear and axial compression during the loading cycle $R$ of $5.0\times10^{-2}$ rad.

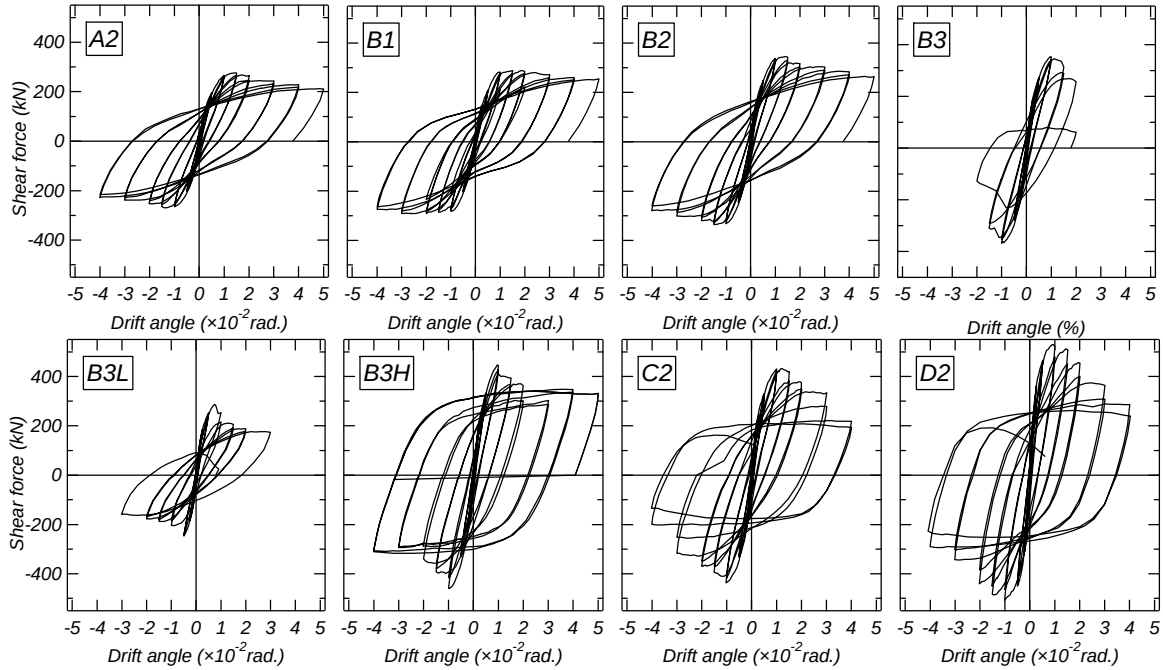


**Figure 3.1** Shear force – drift angle relationships

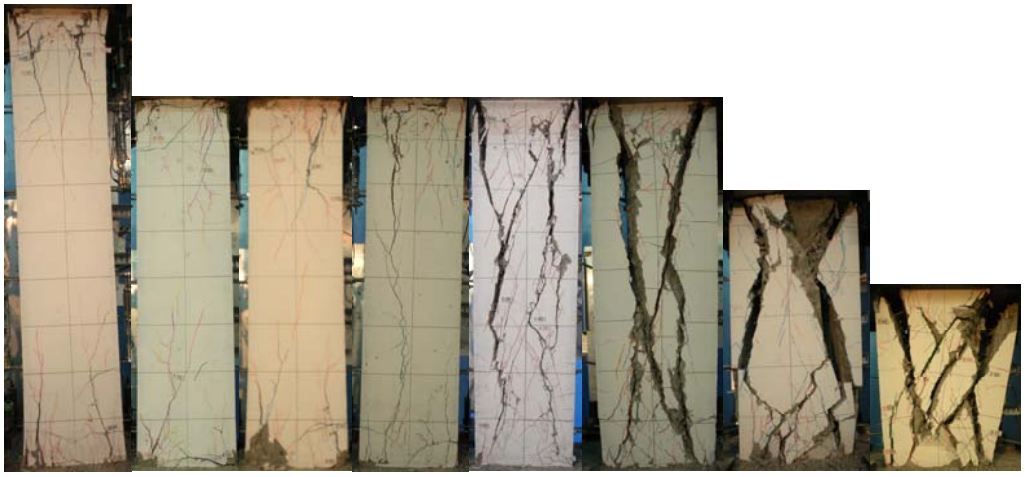


**Photo 3.1** Crack pattern of specimens after loading

In Specimen D2, the initial shear cracks occurred at $R$ of $0.5\text{x}10^{-2}$rad. from the top to bottom of column. At $R$ of $1.0\text{x}10^{-2}$rad. the shear cracks propagated significantly, and the maximum strength was attained. Also, the sign of concrete compressive failure was observed at the both ends and middle of column. After this, with the shear cracks propagation and cover concrete spalling, the strength deteriorated and the specimen was unable to sustain the axial load at $R$ of $5.0\text{x}10^{-2}$rad.

### 3.2. Experimental Results of Phase 2

Shear versus story drift angle relationships of Phase 2 test are shown in Fig. 3.2. Crack pattern on column faces of all specimens at the final loading stage are also presented in Photo 3.2.

In Specimen B30-a, flexural cracks occurred at the lower part of the column at story drift angle $R$ of $0.25\text{x}10^{-2}$rad. The maximum strength was obtained at $R$ of $0.91\text{x}10^{-2}$rad. when the steel yielded. From the Fig. 3.2, it can be seen that sudden strength deterioration occurred at $R$ of $3.0\text{x}10^{-2}$rad.

In Specimen B30-b, at story drift angle $R$ of $0.91\text{x}10^{-2}$rad., the steel yielding occurred and the maximum strength was attained. After this flexural cracks occurred at both ends of column. With the

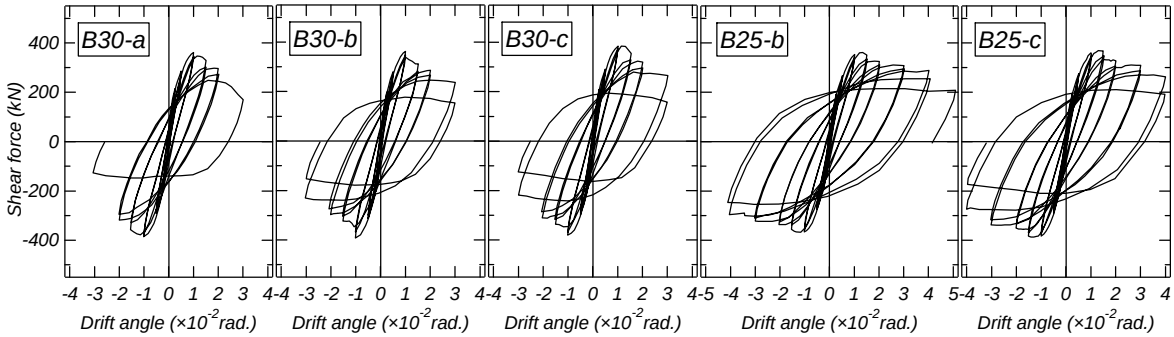


**Figure 3.2** Shear force – drift angle relationships

increase of the story drift angle, sudden strength degradation was observed at the 2nd loading cycle of $R$ of $3.0 \times 10^{-2}$rad. Although there was some improvement on the deformation capacity by band plates, it was not enough to prevent the strength deterioration.

Specimen B30-c showed similar cracks pattern as Specimen B30-b, but with less shear cracks propagation. Besides, no improvement on the deformation capacity was observed due to the band plates.

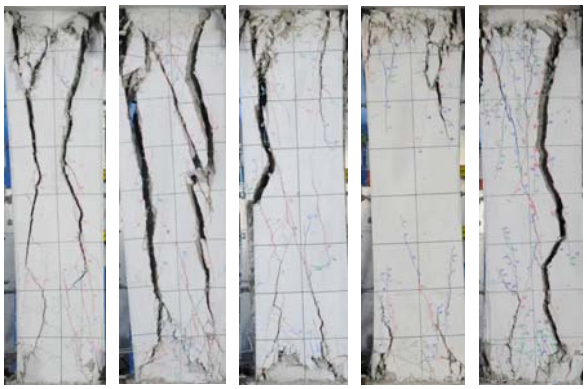

B30-a B30-b B30-c B25-b B25-c

**Photo 3.2** Crack pattern of specimens after loading

Specimen B25-b showed hysteresis loops with better deformation capacity, compared with the Specimens B30-b. The steel yielded at story drift angle $R$ of $0.83 \times 10^{-2}$rad. and the maximum strength was observed at $R$ of $1.34 \times 10^{-2}$rad. After this cycle the strength start to deteriorate. However, compared with specimens with axial load ratio of 0.3, Specimen B25-b did not show significant strength deterioration.

Specimen B25-c showed almost the same hysteresis characteristics as Specimen B25-b, but the strength deterioration was observed at the 2nd loading cycle of $R$ of $4.0 \times 10^{-2}$rad. The yielding of the steel occurred at $R$ of $0.82 \times 10^{-2}$rad., and compared with Specimen B25-b little improvement of the column deformation capacity was observed, in spite of the 100mm width band plates located at both ends of the column.

### 3.3. Experimental Results of Phase 3

Shear versus story drift angle relationships of Phase 3 test are shown in Fig.3.3. Crack pattern of all specimens at the final loading stage are also presented in Photo 3.3.

Shear cracks for Specimen B3F, with fiber contents ratio of 1.5% occurred at almost same loading stage as Specimen B3 with fiber contents ratio of 1.0%. However after R of $1.5 \times 10^{-2}$ rad., the increase of the fiber contributes to control the new cracks occurrence and width expansion. Moreover sudden strength deterioration was not observed.

In Specimen B3MB where steel flange width was larger than Specimen B3, shear cracks propagated at the top of column, at $R$ of $1.0 \times 10^{-2}$rad. Then cracks' widening became obvious at the front face of the specimen along the steel flange face. Even though gradually strength deterioration was observed the specimen showed good hysteresis characteristics. Also, Specimen B3MB-F, with fiber contents ratio of 1.5% showed almost the same failure mode as Specimen B3MB with fiber contents ratio of 1.0%.

As stated above, Comparing Specimen B3 with B3-F, an evident improvement of the deformation

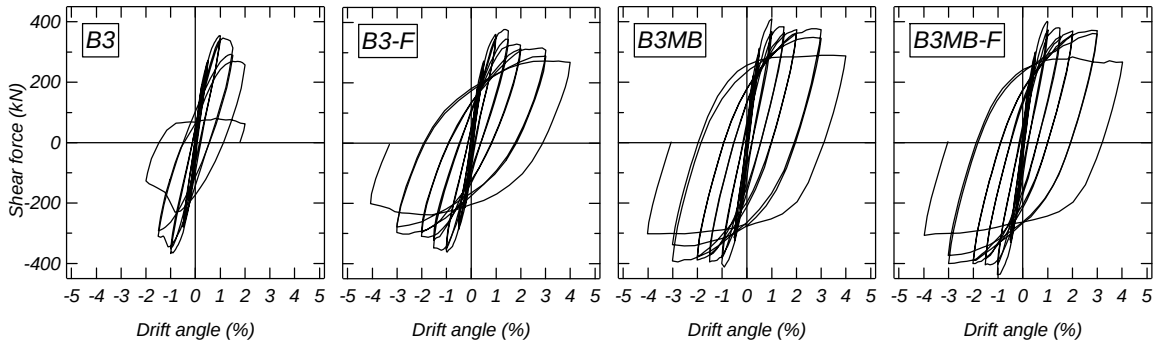


**Figure 3.3** Shear force – drift angle relationships

capacity was observed because of the increment of the fiber contents ratio. However, no improvement was observed in the case of Specimen B3MB-F with 1.5% compared to Specimen B3MB with 1.0%. This is because the larger flange width of steel left a smaller cover concrete and it does not allow the fiber contents to develop their potential to increase the column deformation capacity.

On the other hand, since the flange width of Specimens B3MB and B3MB-F was increased, compared with Specimens B3 and B3-F, the confined concrete area by the steel was also increased. Therefore the deformation capacity improved regardless of the fiber contents ratio.

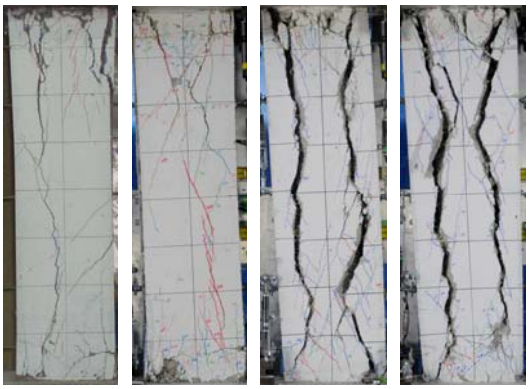

B3 B3-F B3MB B3MB-F

**Photo 3.3** Crack pattern of specimens after loading

## 4. Evaluation of Deformation Capacity of CES Columns

### 4.1 Influence of Each Parameter

The quantification of the influence of fiber contents and flange width to deformation capacity of CES columns will be analyzed. As shown Section 3.3, the deformation capacity of Specimen B3-F, with the fiber content ratio of 1.5%, was obviously improved in comparison with Specimen B3 with 1.0%. However no significant difference was observed between Specimens B3MB-F and B3MB with same flange width but difference fiber content ratio.

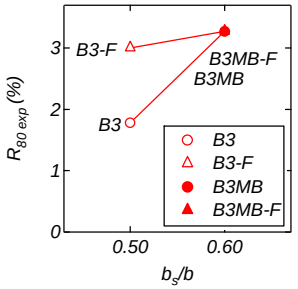


**Figure 4.1** $R_{80\,exp}$-$b_s/b$

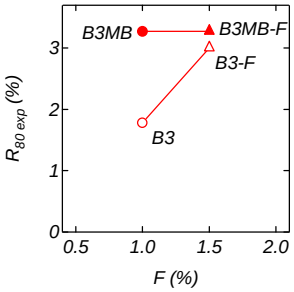


**Figure 4.2** $R_{80\,exp}$-$F$

The relationship between $R_{80exp}$ and flange width ratio $b_s/b$ is shown in Fig. 4.1, where $R_{80\,exp}$ is the drift angle when the shear strength fall to 80% of its maximum value so-called here ultimate drift angle. First the effect of flange width on the ultimate drift angle of CES columns will be examined. The $R_{80exp}$–$b_s/b$ relationship for Specimen B3 and B3MB with the fiber content of 1.0% is written as Eqn. 4.1, and Eqn. 4.2 shows the relationship for B3-F and B3MB-F with 1.5%.

$$R_{80\ exp}=14.9b_s/b-5.7 \quad (4.1)$$

$$R_{80\ exp}=2.7b_s/b+1.7 \quad (4.2)$$

On the other hand, taking only the fiber content ratio as parameter, the $R_{80\ exp}$–$F$ relationships of Specimen B3 and B3-F, Specimen B3MB and B3MB-F are shown in Fig. 4.2 where F is the fiber contents ratio. Now considering the flange width, the relationship between $R_{80exp}$ and $F$ can be written as Eqn. 4.3. That is to say, from Eqn. 4.1, and Eqn. 4.2, the Eqn. 4.3 is equation of the line passing the

two points of (1, 14.9$b_s/b$-5.7) and (1.5, 2.7$b_s/b$+1.7).

$$R_{80\ exp} = (-24.4\ \ b_s/b + 14.6)\ \ F + 39.3\ \ b_s/b - 20.3 \tag{4.3}$$

Table 4.1 shows the three parameters axial load ratio, steel ratio and shear span ratio together with the corresponding drift angles of $R_{80exp}$, $R_{85exp}$ and $R_{90exp}$ for each specimen, where $R_{85exp}$ and $R_{90exp}$ are defined like $R_{80exp}$ as explained above. The relationship between ultimate drift angle and the three parameters will be discussed in the next paragraphs.

Taking the axial load ratio $N/N_0$ as the only parameter, Fig. 4.3(a) shows the relationship between $R_{80exp}$ and $N/N_0$ for Specimens B1, B2, B3, B25-C and B30-a, which have the same steel ratio $A_s/BD$ of 0.0421 and shear span ratio $a/D$ of 2.0. It shows that the ultimate story drift angle $R_{80exp}$ and $N/N_0$ have an almost linear relationship.

Taking the steel ratio $A_s/BD$ as the only parameter, Fig. 4.3(b) shows the relationship between $R_{80exp}$ and $A_s/BD$ for Specimens B3L, B3 and B30H, which have the same axial load ratio $N/N_0$ of 0.3 and shear span ratio $a/D$ of 2.0.It also shows that the ultimate story drift angle $R_{80exp}$ and $A_s/BD$ have an almost linear relationship.

Taking the shear span ratio $a/D$ as the only parameter, Fig. 4.3(c) shows the relationship between $R_{80exp}$ and $a/D$ for Specimens A2, B2, C2 and D2, which have the same axial load ratio $N/N_0$ of 0.3 and steel ratio $A_s/BD$ of 0.0421. It also shows an almost linear relationship between story drift angle $R_{80exp}$ and $a/D$.

As analyzed above, $R_{80exp}$ and the three main parameters of axial load ratio, steel ratio and shear span ratio showed almost linear relationship, which was also confirmed for $R_{85exp}$ and $R_{90exp}$.

A formula that can comprehensively evaluate the deformation capacity taking in to consideration the influence of these parameters of CES columns will be proposed in the next section.

**Table 4.1** Each Parameter & Drift Angle Value

| Specimen | *N/N0* | *As/BD* | *a/D* | $R_{80\ exp}$ | $R_{85\ exp}$ | $R_{90\ exp}$ |
|---|---|---|---|---|---|---|
| B1 | 0.095 | 0.0421 | 2 | 6.43 | 5.26 | 4.21 |
| B2 | 0.188 | 0.0421 | 2 | 4.36 | 3.45 | 2.41 |
| B25-c | 0.218 | 0.0421 | 2 | 3.32 | 2.79 | 1.95 |
| B3 | 0.278 | 0.0421 | 2 | 1.78 | 1.62 | 1.45 |
| B30-a | 0.282 | 0.0421 | 2 | 2.06 | 1.83 | 1.56 |
| B3L | 0.292 | 0.0292 | 2 | 1.26 | 1.11 | 0.97 |
| B3H | 0.300 | 0.0701 | 2 | 2.08 | 1.74 | 1.43 |
| A2 | 0.188 | 0.0421 | 2.5 | 4.48 | 3.61 | 2.80 |
| C2 | 0.192 | 0.0421 | 1.5 | 2.71 | 2.15 | 1.83 |
| D2 | 0.193 | 0.0421 | 1 | 2.36 | 2.07 | 1.81 |
| B3-F | 0.28 | 0.0421 | 2 | 3.10 | 2.18 | 1.75 |
| B3MB | 0.28 | 0.0636 | 2 | 3.27 | 3.15 | 3.03 |
| B3MB-F | 0.28 | 0.0636 | 2 | 3.26 | 3.16 | 3.05 |

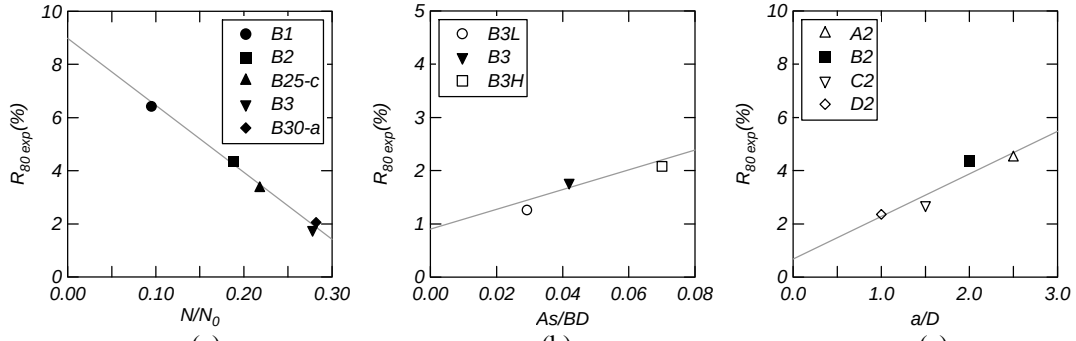


(a) (b) (c)

**Figure 4.3** Relationship between $R_{80exp}$ and parameters

### 4.2 Formulation for the Evaluation of Deformation Capacity

From Fig. 4.3 (a) to Fig. 4.3 (c), the relationship between ultimate story drift angle and the three parameters of axial load ratio, steel ratio and shear span ratio is showed from Eqn.(4.4) to Eqn.(4.6) , respectively.

$$R_{80exp}=-24.6\cdot N/N_0+8.8 \quad (4.4)$$
$$R_{80exp}=18.5\cdot A_s/BD+0.8 \quad (4.5)$$
$$R_{80exp}=1.6\cdot a/D+0.7 \quad (4.6)$$

We assume that,

$$R_{80}=x_1\cdot N/N_0+x_2\cdot A_s/BD+x_3\cdot a/D+x_4\cdot[(-24.4\ b_s/b+14.6)\ F+39.3\ b_s/b]+\ x_5 \quad (4.7)$$

Substituting Eqn. (4.7) into Eqn.(4.3) to Eqn.(4.6), respectively, the following equations can be written

$$(x_1+24.6)\cdot N/N_0 + x_2\cdot A_s/BD+x_3\cdot l/D+ x_4\cdot[(-24.4\ b_s/b+14.6)\ F+39.3\ b_s/b]+x_5-8.8=0 \quad (4.8)$$
$$24.6\cdot N/N_0 +(x_2-18.5)\cdot A_s/BD+x_3\cdot l/D+ x_4\cdot[(-24.4\ b_s/b+14.6)\ F+39.3\ b_s/b]+x_5-0.8=0 \quad (4.9)$$
$$24.6\cdot N/N_0 + x_2\cdot A_s/BD +(x_3-1.6)\cdot l/D+ x_4\cdot[(-24.4\ b_s/b+14.6)\ F+39.3\ b_s/b]+x_5-0.7=0 \quad (4.10)$$
$$24.6\cdot N/N_0+x_2\cdot A_s/BD+x_3\cdot l/D+(x_4-1)\cdot[(-24.4\ b_s/b+14.6)\ F+39.3\ b_s/b]+x_5+20.3=0 \quad (4.11)$$

Since the parameters of $N/N_0$, $A_s/BD$, $a/D$ from Eqn. (4.8) to Eqn. (4.11) are variables, Eqn. (4.7) cannot be determined. Consequently, in order to ignore the effects of the parameters of $N/N_0$, $A_s/BD$, $a/D$, letting $x_1+24.6=0$, $x_2-18.5=0$, $x_3-1.6=0$ and $x_4-1=0$, the value of $x_5$ can be found as -17.23, -17.58, -17.52 and -17.81 from Eqns. (4.8), (4.9), (4.10) and (4.11), respectively. The mean value of $x_5$ is -17.6. If we let $x_5=-17.6$, the equation for the ultimate drift angle $R_{80\ cal}$ can be written as follows.

$$R_{80\ cal}=-24.6\cdot N/N_0\ +18.5\cdot A_s/BD\ +1.6\cdot l/D+(-24.4b_s/b+14.6)\ \cdot F+39.3\ b_s/b\ -17.6 \quad (4.12)$$

Using the same process, $R_{85\ cal}$ and $R_{90\ cal}$ were also analyzed and written as follows

$$R_{85\ cal}=-19.1\cdot N/N_0+13.5\cdot A_s/BD+1.2\cdot l/D+(-11.0\ b_s/b\ +6.6)\ \cdot F+26.2\ b_s/b\ -10.3 \quad (4.13)$$
$$R_{90\ cal}=-14.3\cdot N/N_0+9.3\cdot A_s/BD+0.7\cdot l/D+(-5.5\ b_s/b\ +3.4)\ \cdot F+21.3\ b_s/b\ -7.8 \quad (4.14)$$

### 4.3 Validity Verification of the Deformation Capacity Formulas

Table 4.2 lists the results of $R_{80\ cal}$, $R_{85\ cal}$ and $R_{90\ cal}$ from Eqns. (4.12), (4.13) and (4.14), respectively. From these equations, we can infer that the deformation capacity of CES columns will deteriorate with the increase of axial load ratio, but improve with the increase of steel ratio and shear span ratio.

Fig. 4.4 shows the comparison of calculated and test results. The average of the ratio $n=R_{cal}/R_{exp}$ for $R_{80}$, $R_{85}$ and $R_{90}$ is 0.97, 1.00 and 0.99.with standard deviation of 0.10, 0.09 and 0.10, respectively, the deformation capacity of CES columns can be estimated accurately using the proposed formulation.

**Table 4.2** Calculation *R*esult of $R_{80}$, $R_{85}$ and $R_{90}$

| Specimen | $R_{80\ cal}$(%) | $R_{85\ cal}$(%) | $R_{90\ cal}$(%) | $n_{80}$ | $n_{85}$ | $n_{90}$ |
|---|---|---|---|---|---|---|
| B1 | 6.23 | 5.07 | 3.92 | 0.97 | 0.96 | 0.93 |
| B2 | 3.95 | 3.29 | 2.60 | 0.91 | 0.95 | 1.08 |
| B25-c | 3.21 | 2.72 | 2.17 | 0.97 | 0.98 | 1.11 |
| B3 | 1.74 | 1.58 | 1.31 | 0.98 | 0.97 | 0.91 |
| B30-a | 1.64 | 1.50 | 1.26 | 0.80 | 0.82 | 0.81 |
| B3L | 1.16 | 1.13 | 1.00 | 0.92 | 1.02 | 1.02 |
| B3H | 1.72 | 1.53 | 1.26 | 0.83 | 0.88 | 0.88 |
| A2 | 4.75 | 3.89 | 2.95 | 1.06 | 1.08 | 1.06 |
| C2 | 3.05 | 2.62 | 2.19 | 1.13 | 1.22 | 1.19 |
| D2 | 2.23 | 2.01 | 1.82 | 0.94 | 0.97 | 1.00 |
| B3-F | 2.91 | 2.09 | 1.59 | 0.94 | 0.96 | 0.91 |
| B3MB | 3.55 | 3.34 | 3.05 | 1.09 | 1.06 | 1.01 |
| B3MB-F | 3.58 | 3.36 | 3.09 | 1.10 | 1.06 | 1.01 |
| Average value | | $n=R_{cal}/R_{exp}$ | | 0.97 | 1.00 | 0.99 |
| Standard deviation | | σ | | 0.10 | 0.09 | 0.10 |

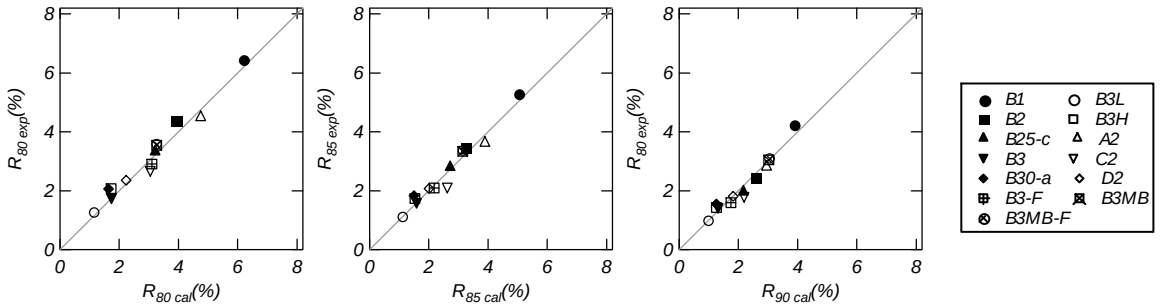


**Figure 4.4** Calculation result of $R_{80}$, $R_{85}$ and $R_{90}$

The validity of the formulation is limited to the experiment data as specified below.

$$0.095 \le N/N_0 \le 0.300, \quad 0.029 \le A_s/BD \le 0.070. \quad 1 \le a/D \le 2.5,$$
$$0.5 \le b_s/b \le 0.6, \quad 1.0 \le F \le 1.5.$$

## 5. CONCLUSIONS

In this research, static loading tests of CES columns with H-shaped steel were carried out. Formulas to evaluate the deformation capacity of CES columns considering the effect of axial load ratio, steel ratio, shear span ratio, fiber contents ratio and flange width are proposed. The following conclusions can be drawn.

1) Deformation capacity of CES columns can be improved by increasing the fiber contents ratio.

2) The increase of the flange width produces an increase of the confined concrete area, which leads to improve the deformation capacity of CES columns. On the other hand, the increase of the flange width produces smaller cover concrete area, therefore when the fiber contents ratio is increased the effect of increasing the deformation capacity is not so significant.

3) The relationship between the parameters (axial load ratio, steel ratio and shear span ratio) and the ultimate drift angle ($R_{80}$, $R_{85}$ and $R_{90}$) was found to be almost linear.

4) Formulas to evaluate the deformation capacity of CES columns are proposed considering the effects of axial load ratio, steel ratio, shear span ratio, fiber contents ratio and flange width. The formulas showed good agreement with the experimental results.

## REFERENCES


Adachi, T., Kuramoto H., Oike, K. and Kawasaki K. (2002). Experimental study on elasto-plastic behavior of composite CES columns using FRC. *Summaries of Technical Papers of Annual Meeting*, Architectural Institute of Japan, **Vol.C-1**, 1025-1026. (in Japanese)

Sasaki, T., Taguchi, T., Kawamoto, T.,Nagata, S., Matsui, T. and Kuramoto, H. (2006). Experimental studies on structural characteristics of CES-columns (Part 1 and 2). *Summaries of Technical Papers of Annual Meeting*, Architectural Institute of Japan, **Vol.C-1**, 1067-1070. (in Japanese)

Fujimoto, T. Kuramoto, H.,and Matsui, T. (2008). Seismic Performance of Columns and Beam-Column Joints in Composite CES Structural System, Proceedings of Fourteenth World Conference on Earthquake Engineering, Beijing, China. Paper ID: **12-03-0071**

Architectural Institute of Japan (2001). *Standard for Structural Calculation of Steel Reinforced Concrete Structures*. (in Japanese)